Appendix

Slice volume derivation

The relative volume of a slice through a p dimensional hypersphere of radius R was previously derived in Laa, Cook, and Valencia (2019). Below we reproduce the calculation for the convenience of the reader. We start with the volume of the hypersphere with radius r in q dimensions:

$$V(r,q) = \frac{\pi^{q/2} r^q}{\frac{q}{2}\Gamma(q/2)}. \tag{1}$$

The variation of the volume with the radius is given as

$$\frac{dV(r,q)}{dr} = 2\frac{\pi^{q/2} r^{q-1}}{\Gamma(q/2)}. \tag{2}$$

The volume in a slice is spherical in the orthogonal space ($p-2$ dimensions) and capturing the full area within the plane. We thus compute it by integrating the product of $\frac{dV(r,p-2)}{dr}$ and the area in the plane parametrised by r. The area in the plane is a circle with radius $\sqrt{R^2-r^2}$. The slice volume is thus calculated as

$$V_{slice}(R,h,p) = \int_0^h \frac{dV(r,p-2)}{dr} V(\sqrt{R^2-r^2},2)dr = \frac{\pi^{p/2}}{\Gamma(p/2)}\frac{h^{p-2}}{p}[pR^2-(p-2)h^2]. \tag{3}$$

The relative volume of the slice given by the fraction

$$V_{rel}(R,h,p) = \frac{V_{slice}(R,h,p)}{V(R,p)} = \frac{h^{p-2}}{2R^p}[pR^2-(p-2)h^2]. \tag{4}$$

Simulated data

The four-dimensional hyperspherical harmonics (Domokos 1967) can be written as

$$Z^m_{n\ell}(\beta,\theta,\phi) = 2^{\ell+1/2}\sqrt{\frac{(n+1)\Gamma(n-\ell+1)}{\pi\Gamma(n+\ell+2)}}\Gamma(\ell+1)\sin^\ell\beta C^{(\ell+1)}_{n-\ell}(\cos\beta)Y^m_\ell(\theta,\phi), \tag{5}$$

where $C^{(\ell+1)}_{n-\ell}$ are the Gegenbauer polynomials and $Y^m_\ell(\theta,\phi)$ are the 3D spherical harmonics. The polynomials are defined over the 4D unit hypersphere S^3 in $\mathbb{R}^4$ and parameterized by three angles: the azimuthal angles ϕ, the 3D zenith (or polar) angle θ and the 4D zenith angle β.

The data sets (A, B) are generated from two of these polynomials. Explicitly they are obtained from,

$$\begin{aligned} \text{Set A}: Z^0_{20} &= \frac{3-4\sin^2\beta}{\sqrt{2}\pi} \\ \text{Set B}: \sqrt{\frac{3}{2}}Z^1_{53} &= \sqrt{\frac{3}{10}}\frac{1}{2\pi}e^{i\phi}\sin^3\beta\left(40\cos^2\beta-4\right)\sin\theta\left(1-5\cos^2\theta\right) \end{aligned} \tag{6}$$

To generate the data sets we start from a uniform sample of points inside a 4-ball of radius one (the inside of the hypersphere S^3) which we then classify into inside or outside points depending on whether r is less than or greater than $|Z^m_{n\ell}(\beta,\theta,\phi)|$. This procedure generates a much larger number of outside than inside points so we collect them separately to obtain reasonably sized samples. The uniform sampling is done in Cartesian coordinates (x,y,z,t) which are then transformed to hyper-spherical coordinates $(r\cos\beta, r\sin\beta\cos\theta, r\sin\beta\sin\theta\cos\phi, r\sin\beta\sin\theta\sin\phi)$.

Radial CDF of projected hyperspheres

The radial CDF used throughout this work can be derived by calculating the fraction of the projected volume within a circle of radius r. The volume of a p dimensional hypersphere with radius R is

$$V(p, R) = \frac{2\pi^{p/2}R^p}{p\Gamma(p/2)} \tag{7}$$

and the projected volume *outside* a circle of radius r is

$$V_{outside}(r, p, R) = \int_r^R V(p-2, \sqrt{R^2-\rho^2})2\pi\rho d\rho = \frac{\pi^{p/2}(R^4 - r^2R^2)^{p/2}}{R^p\Gamma(p/2+1)}. \tag{8}$$

The projected volume *inside* the circle is given by

$$V_{inside}(r, p, R) = V(p, R) - V_{outside}(r, p, R), \tag{9}$$

and we therefore get the relative volume within the circle (and thus the radial CDF) as

$$F(r, p, R) = \frac{V_{inside}(r, p, R)}{V(p, R)} = 1 - \left(1 - \left(\frac{r}{R}\right)^2\right)^{p/2}. \tag{10}$$

Squared masses in the two-Higgs-doublet model

Following Gunion and Haber (2003) we compute the squared masses as

$$\begin{aligned}
m_h^2 &= \frac{v^2}{\sin(\beta-\alpha)}\left(-\lambda_1\cos^3\beta\ \sin\alpha + \lambda_2\sin^3\beta\cos\alpha + \frac{\lambda_{345}}{2}\ \cos(\beta+\alpha)\sin(2\beta)\right) \\
m_H^2 &= \frac{v^2}{\cos(\beta-\alpha)}\left(\lambda_1\cos^3\beta\ \cos\alpha + \lambda_2\sin^3\beta\sin\alpha + \frac{\lambda_{345}}{2}\ \sin(\beta+\alpha)\sin(2\beta)\right) \\
m_{H^\pm}^2 &= \frac{v^2}{\sin(2(\beta-\alpha))}\left(-\sin(2\alpha)\ (\lambda_1\cos^2\beta - \lambda_2\ \sin^2\beta) + \lambda_{345}\ \sin(2\beta)\cos(2\alpha) - \frac{\lambda_{45}}{2}\ \sin(2(\beta-\alpha))\right) \\
m_A^2 &= \frac{v^2}{\sin(2(\beta-\alpha))}\left(\sin(2\alpha)\ (-\lambda_1\cos^2\beta + \lambda_2\ \sin^2\beta) + \lambda_{345}\ \sin(2\beta)\cos(2\alpha) - \lambda_5\sin(2(\beta-\alpha))\right)
\end{aligned} \tag{11}$$

where we have used the shorthand notation $\lambda_{ij\ldots} = \lambda_i + \lambda_j + \cdots$ and the constant $v \approx 246$~GeV sets the scale for the masses.

Additional application: PDFSense data

As similar example, but with different behavior, is given by the decision boundaries of a classification model for the PDFSense dataset. This data has 4021 observations in a 56 dimensional parameter space, that are grouped into 3 classes (Wang et al. 2018). Following the analysis in Cook, Laa, and Valencia (2018) we only consider the first six principal components, and train an svm classification model with radial kernel. We again use classifly and select the resulting sample points inside a 6D hypersphere after individual centering and scaling each of the variables.

For this example, the classifier wraps tightly around two of the groups (DIS and jets), and most of the space is filled by the third group (VBP). We select only the samples predicting the VBP class, generating a sample with a small hollow region to be found by section pursuit. We again use the index with polar binning, with 5 equidistant radial bins and 8 angular bins. We set $q = 1$ and use the tourr function search_better to find the view with the maximum index value.

The result is shown in Fig. 1, comparing the starting projection (top row) and the final view (bottom row). In the final slice view of the classifier predictions we see the decision boundaries between the three classes.

The different regions are hidden in the projection of the classifier and of the data. In this case the svm model uses additional information from the orthogonal directions to separate the three classes. By looking at the final slice from section pursuit we have obtained a conditional view that allows us to resolve the resulting boundary.

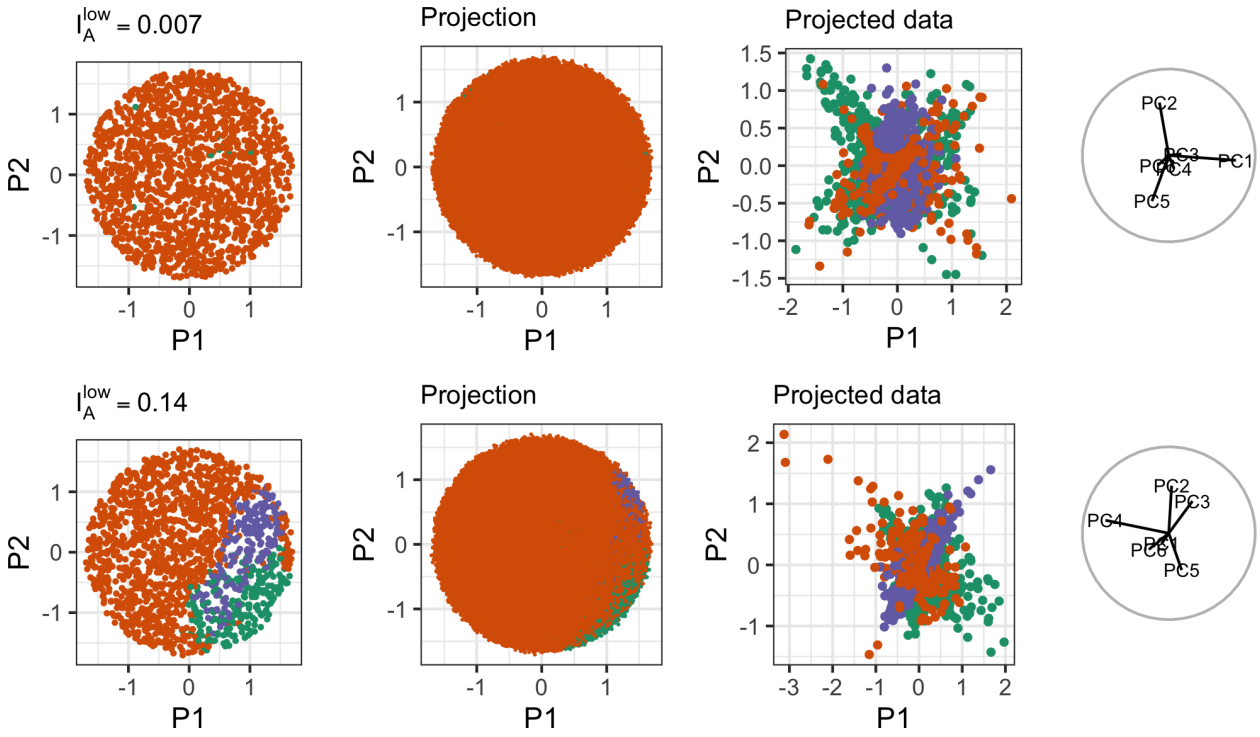

Figure 1: SVM classification of the PDFSense data, with predicted classes mapped to color. The first row shows a random starting projection, the second row is the final projection obtained via section pursuit on the second class shown in orange. The first and second column show the predicted class label from the svm in a thin slice and a projection. The third column shows the projected data in the same plane, and the last column shows the axes of the corresponding projection.

Cook, Dianne, Ursula Laa, and German Valencia. 2018. "Dynamical projections for the visualization of PDFSense data." *Eur. Phys. J.* C78 (9): 742. https://doi.org/10.1140/epjc/s10052-018-6205-2.

Domokos, G. 1967. "Four-Dimensional Symmetry." *Phys. Rev.* 159 (5): 1387. https://doi.org/10.1103/PhysRev.159.1387.

Gunion, John F., and Howard E. Haber. 2003. "The CP conserving two Higgs doublet model: The Approach to the decoupling limit." *Phys. Rev.* D67: 075019. https://doi.org/10.1103/PhysRevD.67.075019.

Laa, Ursula, Dianne Cook, and German Valencia. 2019. "A Slice Tour for Finding Hollowness in High-Dimensional Data." https://arxiv.org/abs/1910.10854.

Wang, Bo-Ting, T. J. Hobbs, Sean Doyle, Jun Gao, Tie-Jiun Hou, Pavel M. Nadolsky, and Fredrick I. Olness. 2018. "Mapping the sensitivity of hadronic experiments to nucleon structure." *Phys. Rev.* D98 (9): 094030. https://doi.org/10.1103/PhysRevD.98.094030.